Journal of Hepatocellular Carcinoma

Dovepress
Taylor & Francis Group

Open Access Full Text Article

ORIGINAL RESEARCH

Beta-Catenin Mutations Can Impact on the Interplay Between Tumor and Immune Cells and Hepatic Microbiota in Hepatocellular Cancer

Yu Ota[1], Julia Driscoll[1], Anneliese R Hill[2], Irene K Yan[1], Tushar Patel[1]

[1]Department of Transplantation, Mayo Clinic, Jacksonville, FL, USA; [2]Cytometry and Cell Imaging Lab, Mayo Clinic, Jacksonville, FL, USA

Correspondence: Tushar Patel, 'Division of Gastroenterology and Hepatology, Department of Transplantation, Mayo Clinic, 4500 San Pablo Road, Jacksonville, FL, 32224, USA, Email patel.tushar@mayo.edu

Introduction: Emerging evidence links alterations in the tumor microbiome to therapeutic responses to immunotherapy. Alterations in β-catenin are among the most frequently observed oncogenic drivers of hepatocarcinogenesis and are associated with T-cell exclusion. However, their effect on the immune cell environment and microbiome in hepatocellular cancer is not well understood. We hypothesized that β-catenin could modulate the immune microenvironment through alterations in the secretome and release of extracellular vesicles (EV) that mediate tumor and immune cell interactions and increase tumor growth within regions with attenuated immune activity and reduced microbial diversity.

Methods: We used a synthetic transgenic murine model of β-catenin-driven hepatocarcinogenesis to analyze microbiome composition, diversity, and immune cell profiles in vivo. Tumor and stool samples were collected from mice with early- or late-stage hepatocellular carcinoma and were used for profiling.

Results: The microbiome associated with intrahepatic tumors differs from that in non-tumoral regions, normal liver tissues, and gut tissues. Constitutive β-catenin expression modulates lipopolysaccharide-mediated signaling in macrophages and alters the secretion of immunomodulatory chemokines and cytokines. Tumoral immune cell profiles differed from those in hepatic tissues. EV-mediated signaling between immune cells and epithelial cells with mutant β-catenin and immune cells modulates immune cell populations in vitro and in vivo.

Conclusion: Mutations in β-catenin can drive immune responses through EV-based tumor cell-immune cell interactions to modulate both the tumor microflora and immune microenvironment. A potential strategy to augment responses to immunotherapy for hepatocellular cancer could target these interactions to restore microbial diversity or immune cell infiltration within the tumor microenvironment.

Keywords: beta-catenin, extracellular vesicles, tumor microbiome, immune escape, tumor microenvironment

Introduction

A variety of constituents of the local tumor microenvironment (TME) can regulate immune responses both locally and systematically through intracellular signaling mediated by extracellular vesicles. These include normal tissue as well as tumor, stromal, immune, and microbial cells within the TME. In addition to tumor surveillance, the immune system plays an essential role in the response to exogenous stimuli, such as microbes. Although recent data have emphasized the clinical relevance of the tumor microbiome, the inter-relationships between transformed cells, the microbiome, and immune cell functions within the local TME remain undefined. Independent of the effects of tumor cells, the microbiome within tissues can modulate the local microenvironment by influencing immune cell activation and function, which could impact tumor formation or progression. In regions of low microbial diversity, for example, relatively low antigenic or adjuvant immune stimulation and activity could in turn contribute to attenuated immunosurveillance responses that promote tumor growth. Conversely, oncogenic changes within tumor cells can modulate the local TME and immunity

Received: 22 February 2025
Accepted: 19 July 2025
Published: 1 August 2025

through alterations in the cellular secretome and the release of extracellular vesicles that mediate cellular interactions between the tumor and immune cells within the TME.[1]

Therapies that inhibit pathways that reduce the antitumor immune response have shown great promise in some cancers. However, even though some immune checkpoint inhibitors have been approved for primary liver cancers such as hepatocellular cancer (HCC), their response to immune blockade is poor. These cancers are generally associated with a lower infiltration of T cells within the TME which manifest as a "cold" or "T-cell-non-inflamed" phenotype. This phenotype has been associated with lower efficacy of immunotherapies such as immune-checkpoint blockers in HCC as well as in many other cancers.[2,3] Understanding the mechanisms underlying the lack of pre-existing tumor T-cell infiltration is key to improving the therapeutic responses.[4] HCC is also frequently associated with gut dysbiosis and alterations in the gut microflora are associated with its formation. Thus, the gut microbiota can also influence anticancer therapies that seek to boost immunosurveillance.

In HCC, approximately 30% of tumors fall within an immune exclusion class characterized by T-cell exclusion from the TME and CTNNB1 mutations.[5] β-Catenin alterations are among the most frequently observed oncogenic alterations in HCC. However, the role of β-catenin mutations in hepatocytes, their impact on immune cell exclusion or function, and the microflora within the local TME are not well established. Mutations in CTTNB1 are associated with lower leukocyte counts in different cancer types.[6] Moreover, the activation of tumor-intrinsic Wnt/β-catenin signaling correlates with an absence of T-cell infiltration in some cancers and is frequently observed and correlated with non-T-cell-inflamed tumors.[7–9] These tumors exhibit innate resistance to anti-PD-1 or PDL-1 inhibitors.[2,3,10] The associated immune exclusion may reflect alterations in the TME. In these settings, immune exclusion may arise from the repression of key chemokines by activated β-catenin signaling and the subsequent failure to recruit $CD8^+$ T cells, resulting in resistance to checkpoint blockade.

To understand the interrelationships between the immune cell environment and tumor microbiome and tumor cell-immune cell interactions mediated by extracellular vesicle (EV) based signaling, we examined the effects of mutant β-catenin in vitro using a synthetic transgenic model in vivo. We hypothesized that regions with a higher microbial diversity and greater immune activity would have a relatively lower tumor burden. Our goals were to understand if HCC formation was reflected in alterations in the hepatic microbiome and to identify if (a) specific microbial profiles were associated with HCC, (b) the relationship between these profiles and immune suppression, and (c) the association between the hepatic microbiome and tumor formation. We systematically analyzed the microbiome composition, diversity, and immune cell profiles in tumoral and non-tumoral regions within the context of β-catenin mutations and the impact of tumor cell-immune cell signaling on driving immune responses.

Materials and Methods

Plasmids and Lentiviral Vectors

β-catenin (S33Y) -pcw107-V5 was a gift from Dr. David Sabatini and Kris Wood (Addgene plasmid #64616), and pcw107 was a gift from Dr. John Doench and David Sabatini (Addgene plasmid #62511). HEK 293T cells (3 × 106 cells) were seeded onto a 100 mm dish, and co-transfected with 3 μg of transfer expression plasmid DNA (mutant β-catenin lentivirus or empty lentivirus), 0.3 μg of VSV-G envelope expressing plasmid pMD2.G (gift from Dr. Didier Trono, Addgene plasmid #12259) and 2.7 μg of packaging plasmid psPAX2 (gift from Dr. Didier Trono, Addgene plasmid #12260) using Lipofectamine 2000 (Invitrogen, cat no. 11668030, Carlsbad, CA, USA). The lentivirus-containing supernatant was collected 48 h after transfection and used in the subsequent experiments.

Cells and Cell Culture

RAW264.7 mouse macrophage, AML 12 mouse hepatocyte, and HEK 293T human embryonic kidney cells were obtained from ATCC (ATCC Manassas, VA, USA). RAW264.7 and HEK 293T cells were maintained in Dulbecco's Modified Eagle's medium (DMEM) supplemented with 10% fetal bovine serum (FBS) and 1% penicillin-streptomycin. AML12 cells were cultured in DMEM/F-12 medium (1:1) containing 10% FBS, 1% penicillin-streptomycin, 10 μg/mL insulin, 5.5 μg/mL transferrin, 5 ng/mL selenium, and 40 ng/mL dexamethasone. All cells were cultured at 37°C and 5%

CO_2. For the generation of stable mutant β-catenin expressing cells, AML12 cells (1×10^5 cells) were seeded in a 6-well plate and allowed to attach overnight at 37°C. The lentivirus-containing supernatant and polybrene were added to each well and incubated for 6 h, after which the medium was replaced with complete medium. After 2 days, transduced cells were expanded to a 10 cm dish in complete medium containing puromycin (0.1 μg/mL), and the medium was changed every 3 days for 2 weeks. Isolated puromycin-resistant clones were then selected and amplified. Stable mutant β-catenin-expressing cell lines, or controls transduced with an empty lentiviral vector, were used for further experiments.

Co-Culture Studies

For lipopolysaccharide (LPS) stimulation, RAW264.7 cells (3×10^6 cells) were seeded into a 100 mm dish and incubated overnight, and then incubated for 12 hours with 200ng/mL of lipopolysaccharide (LPS from Escherichia coli O55:B5; cat no. L6529, Sigma, St Louis, MO). LPS-stimulated RAW264.7, were harvested, cultured alone (monoculture), or co-cultured with AML12 cells. LPS-stimulated RAW264.7 cells (3×10^5 cells) were seeded into a 6-well plate, while AML12 control cells or AML12 mutant β-catenin cells (3×10^5 cells/insert) were plated on a Transwell insert with a membrane pore size of 0.4 μm (Cat no. 353090 Thermo Fisher Scientific, Waltham, MA), and placed within the co-culture plates containing RAW264.7 cells, and then cultured in EV-depleted medium for 48 hours. Culture supernatants from the basolateral side were collected for protein measurements or extracellular vesicle isolation. The cultured RAW264.7 cells were harvested for subsequent studies for total RNA isolation and RT-PCR.

Isolation of Extracellular Vehicles (EVs)

Cell culture supernatants were collected and centrifuged at 300 × g for 5 min, then at 2,000 × g for 30 min at 4°C. EVs were then isolated using the KrosFlo KR2i Tangential Flow Filtration (TFF) System (Repligen; Waltham, MA) using a modified polyethersulfone 0.5 mm filter with a 10 kDa molecular weight cutoff (cat no. C02-E010-05-S; Repligen, Waltham, MA). The suspension was continuously circulated through the membrane filter system, concentrated to a volume of 2 mL, diluted five times with PBS, and further concentrated to achieve a final volume of 2 mL. The resulting EV were further concentrated by ultracentrifugation at 100,000 x g for one hour and 10 min at 4°C. EV pellets were re-suspended in small volumes of PBS and quantified using nanoparticle tracking analysis (NTA, Nanosight LM10, Malvern, UK).

Protein Extraction and Western Blotting

Total protein was extracted from cultured cells or EVs using the M-PER Mammalian Protein Extraction Reagent (Thermo Fisher Scientific). The protein concentrations were determined using a bicinchoninic acid (BCA) assay protein assay kit (Thermo Fisher Scientific). Equivalent amounts of protein were mixed with 4 × NuPAGE LDS Sample Loading Buffer (Thermo Fisher Scientific), separated on NuPAGE Bis-Tris Mini Gels (Thermo Fisher Scientific), and transferred onto nitrocellulose membranes. The membranes were blocked with Odyssey blocking buffer (LI-COR, Lincoln, NE) for 1 h at room temperature and then incubated overnight at 4°C with the indicated primary antibodies listed in Supplementary Table 1. Protein expression was visualized and quantified using the Odyssey Imaging system (LI-COR).

Cytokine/Chemokine Assays

Cell culture supernatants were collected and centrifuged at 300 × g for 5 min, then at 2,000 × g for 30 min at 4°C. Samples were stored at −20°C until analysis. Multiplex assays for the selected cytokines and chemokines were performed using Eve Technologies (Calgary, Canada).

Synthetic Transgenic Model of HCC

Six-week-old male and female Friend virus B (FVB) mice were obtained from Jackson Laboratory (Bar Harbor, ME). The HCC mouse model was generated by co-expression of c-tyrosine-protein kinase Met (c-MET) and mutant ΔN90-β-catenin in mouse livers using a sleeping beauty (SB) transposon/transposase system. Plasmids were amplified using One Shot TOP10 chemically competent Escherichia coli cells (Thermo Fisher Scientific) and further purified using the PureYield Plasmid Maxiprep System (Promega, Madison, WI, USA). Hydrodynamic injections were performed as previously described.[11] For generation of tumors, 22.5 μg pT3-EF1a–c-MET (human), 22.5 μg

pT3-EF1a–ΔN90-β-catenin (human), 5 μg pT3–Gaussia luciferase, and 5 μg SB transposase diluted in 2 mL TransIT-EE Hydrodynamic Delivery Solution (Mirus Bio) were administered to male or female mice (n=14 each) by hydrodynamic injection of the tail vein: for controls, 22.5 μg pT3-EF1a–c-MET (human), 5 μg pT3–Gaussia luciferase, and 5 μg SB transposase diluted in 2 mL TransIT-EE Hydrodynamic Delivery Solution were administered to male and female mice (n=9 each). For effective hydrodynamic injection, the solution was injected within a 7 second period. To monitor tumor growth, venous blood was collected from the tail vein 4, 7, 11, and 15 weeks after hydrodynamic injection. The blood samples were coagulated at room temperature for 15 min and subsequently centrifuged at 10,000 rpm for 5 min. Serum was collected and a luciferase assay was performed according to the manufacturer's protocol (cat no. 16160, Thermo Fisher Scientific, Waltham, MA, USA). Mice were sacrificed when tumor luciferase activity was less than 1,000,000 RLU or greater than 1,000,000 RLU, corresponding to early and advanced HCC, respectively. The livers were harvested and histological examination, gene expression profiling, hepatic microbiota screening, and immune profiling were performed. No animal was excluded from the analysis.

All animals received humane care, and all studies involving animals were performed according to the protocols approved by the Mayo Clinic Institutional Animal Care and Use Committee (# A00005435-20). Mice were housed in individually ventilated cages (Allentown Inc., Allentown, NJ, USA) with bed-o'cobs bedding (Anderson's, Maumee, Ohio, USA) and nestles for enrichment. The mice were maintained under a 12-hour light/dark cycle and fed food (Pico Diet 5053 LabDiet, St. Louis, MO, USA) and water ad libitum.

Isolation of Hepatic Non-Parenchymal Cells

A mouse with early HCC was sacrificed, and the liver was harvested. Liver tumor tissues and adjacent non-tumor tissues were separated. The tissues were minced into 1 mm sized pieces and passed through a 70 μm cell strainer. The cell suspensions were then incubated with 1.0mg/mL of collagenase IV (Fisher, #17104019) for 30 min at 37°C and then centrifuged at 50 × g for 5 min at 4°C to pellet the hepatic parenchymal cells. The supernatants were transferred to new tubes and centrifuged at 180 × g for 10 min at 4°C. The supernatants were discarded, and the pellets were collected for analysis by mass cytometry.

Histology and Immunohistochemistry

Liver tissue staining for hematoxylin and eosin (H&E) and immunohistochemical analyses were performed using the Mayo Clinic Florida Cancer Biology Histology Shared Resource. Briefly, slides were de-paraffinized and hydrated with distilled water, and antigen retrieval was performed by soaking the slides in ethylene diamine tetraacetic acid (EDTA) in a 100 °C steamer for 25 min. Immunohistochemistry was performed using the following primary antibodies: anti-CD8 (1:2000 dilution; cat. ab209775, Abcam) and anti-LPS (1:50 dilution; cat. LS-C375096-200, LSBio, Seattle, WA). The tissues were subsequently stained with a pre-diluted EnVision HRP-labeled polymer anti-rabbit secondary antibody (Cat No. K4003, Dako, Carpinteria, CA). H&E staining was performed using the Mayo Clinic Florida Histology Shared Resource.

Genomic DNA Extraction

The livers were harvested from six c-MET control mice and seven mice with early (n=3) or advanced (n=4) HCC. Liver tissue DNA was immediately extracted from the c-MET control mouse liver tissue samples and from the HCC mouse tumor and adjacent non-tumor tissue samples using the PureLink Genomic DNA Kit (cat no. K182001, Life Technologies, Carlsbad, CA). For DNA isolation, stool samples were collected 10–12 weeks after hydrodynamic injection. Samples were immediately stored at −20°C until DNA extraction. DNA was extracted using the QIAamp Fast DNA Stool Mini Kit (cat. no. 51604, Qiagen, Germany). Following isolation, DNA was stored at −20°C until further analysis.

16S rRNA Gene Sequencing

DNA samples were subjected to 16S rDNA sequencing by GENEWIZ LLC (South Plainfield, NJ, USA). To prepare the DNA library, the variable regions (V3, V4, and V5) of the prokaryotic 16S rDNA were amplified by polymerase chain

reaction (PCR) using proprietary V3-V5 specific primers. DNA libraries were multiplexed and sequencing of the 16S rDNA variable region was performed using an Illumina MiSeq instrument. The data were pre-processed using Cutadapt (v1.9.1), Vsearch (v1.9.6), and Qiime (v1.9.1) to improve quality and accuracy prior to bioinformatics analysis. For each read pair, two overlapping sequences were merged if the overlap was at least 20bp long. Undetermined bases, primers, and adapter sequences were removed from merged sequences. Quality filtering was performed and only sequences with a Q score >20 and length > 200bp were retained. The sequences were compared with the UCHIME Gold database to detect and remove chimeric sequences. Unique sequences were extracted from the optimized sequences using read count information. The sequences were clustered according to their similarity to operational taxonomic units (OTU), using a threshold of 97%. The number of species in the microbial communities was estimated using the ACE and Chao1 indices. Alpha diversity was calculated using Shannon and Simpson indices. Beta diversity was calculated using UniFrac analysis, and absolute genus abundance was visualized using principal component analysis (PCA) based on the sample similarity coefficient matrix.

Isolation of Mouse Splenocytes for Immune Cell Profiling

Male C57BL/6 wild-type mice were obtained from Jackson Laboratory (Bar Harbor, ME, USA). For immune cell profiling, EV (1.0×10^{10} particles) were administered to male C57BL/6 mice via tail vein injections. Mice were sacrificed 4 h after the injection, and their spleens were harvested. The spleens were macerated over a 70 μm cell strainer in a tube containing wash buffer consisting of ice-cold PBS supplemented with 0.6% sodium citrate (cat no. S-4641 Sigma, St. Louis, MO, USA), and 0.1% bovine serum albumin (cat no. sc-2323 Santa Cruz Biotechnology; Dallas, TX). The splenocytes were centrifuged at 180 × g for 5 min at 4°C. The supernatants were discarded and the pellets were re-suspended in wash buffer. This process was repeated twice, after which the isolated splenocytes were re-suspended in FBS supplemented with 10% DMSO and stored overnight at −80°C. The harvested splenocytes were used for the mass cytometry experiments.

Mass Cytometry

Cells were re-suspended at a concentration of 4×10^6 cells / 150μL in MaxPar cell staining buffer (CSB; cat no. 201068; Fluidigm, San Francisco, CA, USA). Cisplatin labeling was used to identify dead cells. The samples were stained with Cell-ID Cisplatin (cat no. 201064, Fluidigm, San Francisco, CA, USA) and incubated at room temperature for 5 min. To block Fc receptors, 2.5% heat-inactivated mouse serum was prepared in CSB as previously reported.[12] The samples were incubated with 50 μL mouse serum solution for 10 min at room temperature. After Fc blocking, the samples were stained with 50 μL of the respective antibody cocktail (Supplementary Table 2) and then fixed with 1.6% paraformaldehyde solution (cat no. 28906, Thermo Fisher Scientific, Waltham, MA). To identify the nucleated cells, samples were incubated overnight at 4°C with 1 mL of intercalation solution (Cell-ID Intercalator-Ir; cat no. 201192A,Fluidigm,San Francisco, CA) diluted 1:1,000 in MaxPar Fix and Perm buffer (Fluidigm, #201067), and then centrifuged at 800 × g for 5 min at 4°C and re-suspended in the MaxPar cell acquisition buffer (CAS; Fluidigm, #201237). A 1:10 solution of EQ equilibration beads (Fluidigm, #201078) was prepared in CAS and used to resuspend the samples to achieve a final concentration of 1×10^6 cells/mL. Single-cell suspensions were obtained by passing the samples through a 35 μm filter prior to data acquisition. The data were acquired using Fluidigm Helios CyTOF and exported as a flow cytometry standard (.fcs) files. Before data analysis, the samples were normalized according to the calibration beads, and pre-gating was performed to select the live singlet cells. The samples were subsequently concatenated, and gating was performed using FlowJo software. The .fcs files were analyzed using the CyTOFkit package in RStudio to generate tSNE plots.

Statistical Analysis

All analyses were performed using GraphPad Prism 7 (GraphPad Software Inc., San Diego, CA, USA). Data are expressed as the mean ± standard error of at least three replicates. The differences between two groups were compared using an unpaired two-tailed Student's *t*-test. Statistical significance was set at $p < 0.05$.

Results

Are Microbial Products Detectable in HCC?

We began our studies using an in vivo model of HCC induced by hepatic expression of mutant β-catenin. This model involves hydrodynamic injection of sleeping beauty transposase-mediated delivery of mutant β-catenin and c-MET into the liver. We previously used this model to demonstrate the relative refractoriness to immunotherapy, as well as its dependency on mutant β-catenin.[13,14] In the presence of a therapeutic blockade of β-catenin administered via biological nanotherapeutics, we observed an increase in sensitivity to immunotherapy. This establishes the dependency of oncogenic β-catenin expression on tumor formation and progression. We hypothesized that tumor formation in this model was related to local TME factors. First, we analyzed the expression of lipopolysaccharide (LPS), a cell wall product of gram-negative bacteria, which is highly prevalent in the gut and is related to the gut microflora. LPS is also present in the portal vein, particularly under inflammatory stress resulting from disruption of intestinal epithelial integrity. We performed IHC for LPS and CD8 in the patients with advanced HCC (Figure 1). LPS was present in the tumor tissues of these mice. As expected, there were very few $CD8^+$ T cells observed, consistent with these representing "cold" tumors. The $CD8^+$ count was low in early HCC, but higher in more advanced HCC. Moreover, we observed that regions of CD8 expression were associated with LPS.

Are There Changes in the Microbiome Diversity and Composition Associated with Tumors?

Having demonstrated the presence of LPS, we next examined whether there were any microflora within the liver tissues or whether the observed LPS arose from the gut microflora. For analysis of the hepatic microbiome, tissue DNA samples were obtained from control mice (n = 6) or from tumor tissues or adjacent non-tumoral tissues from HCC-bearing mice (n = 7) and were used for 16S rRNA sequencing. Assessment of the tumor microbiome in tumor and non-tumoral regions showed no significant differences in alpha diversity in the tumor, adjacent non-tumor, and control liver tissues (Figure 2). To identify differences in microbiome ecosystems between the control and HCC liver tissues, principal component analysis (PCA) plots were constructed with 30 operational taxonomic unit (OTU) clusters or 18 genera. The HCC hepatic microbiomes exhibited similar OTU and genera signatures that differed from those of the non-HCC livers. These differences were not significant (OTU PCA plot, p=0.128; genus PCA plot, p=0.34). An increase in *Escherichia, Atopobium, Megsphera, Acenitobacter* and *Staphylococcus*, but a decrease in *Desufobacter, Wolbachia*, Serratia, *Vibrio, Pseudomonas* and *Rothia* was noted in HCC mouse livers. These results indicated that the microbiome associated with HCC mouse tissues is distinct from that associated with normal mouse tissues.

Does the Tumor Microbiome Reflect the Gut Microbiome?

For the analysis of the gut microbiome, stool samples were obtained from control mice (n = 6) and HCC-bearing mice (n = 7). Sequencing of 16S rRNA sequencing was performed on stool DNA samples, and the alpha and beta diversities of the microbiota were assessed. Compared to control mice, a higher alpha diversity in the gut microbiome was noted in stool samples from mice with HCC (Figure 3). To evaluate beta diversity in the gut microbiota, principal component analysis (PCA) plots were generated using 23 OTU clusters or 15 genera. Analysis of OTU cluster abundance revealed differences in the gut microbiome signature between control and HCC-bearing mice; however, these differences were not significant (p=0.05). An increase in *Butyricicoccus* and decrease in *Ruminococcus* and *Lactobacillus* were observed in the gut microbiomes of HCC mice. To assess whether the differences in the gut microbiome reflected those in the liver microbiome, we compared the abundance of these genera in the gut to that in the liver. Increases in several genera were observed in the gut microbiomes of HCC mice, whereas decreases in *Clostridium, Escherichia* and *Tenacibaculum* were noted in the gut microbiomes of HCC mice (Figure 4). Compared with the liver microbiome, the gut microbiome of tumor-bearing mice also exhibited an overall lower biodiversity. These results indicate that the tumor microbiome differs from the gut microbiome.

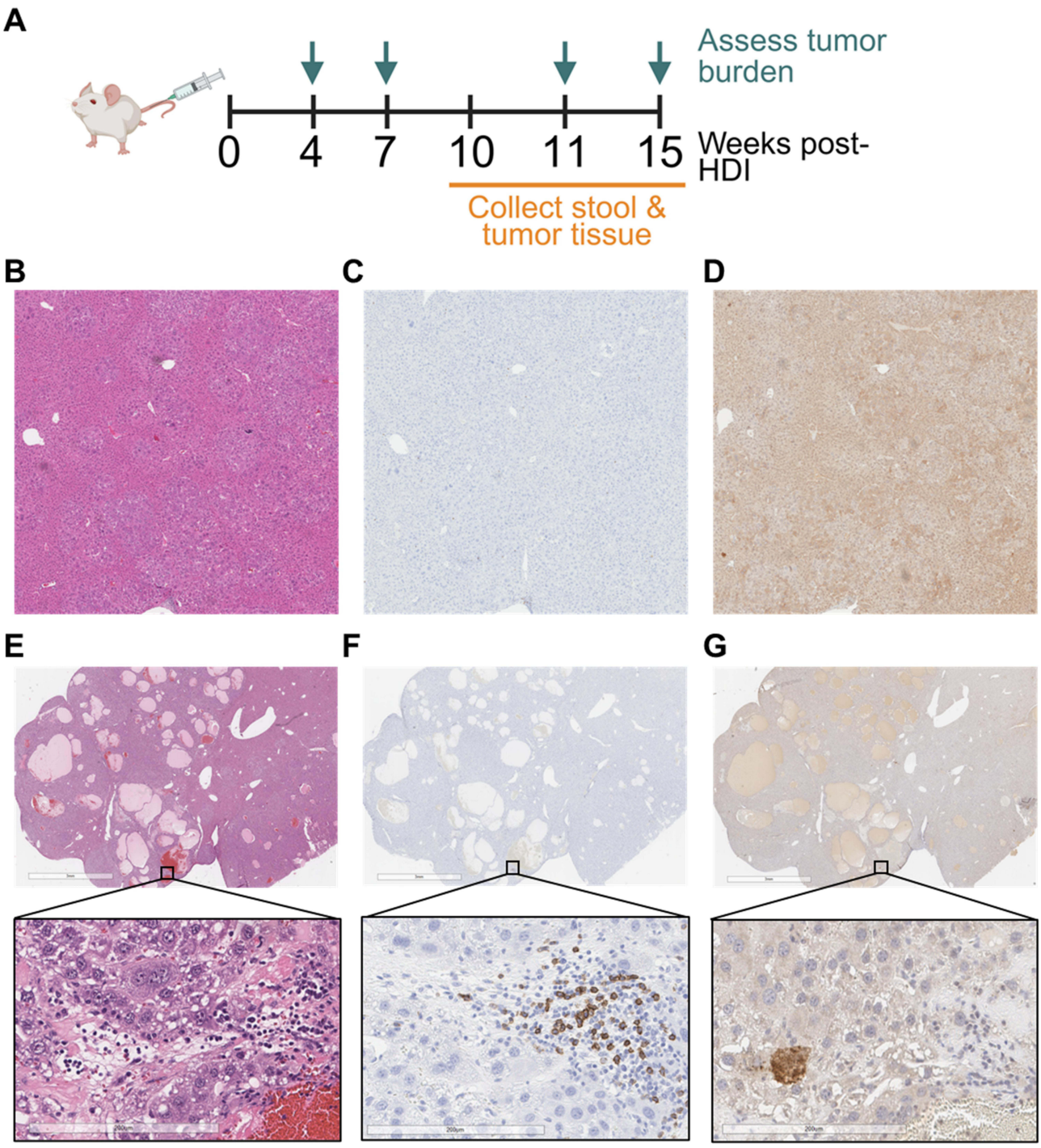

Figure 1 Experimental model of liver cancer. (**A**) A synthetic transgenic model of HCC was established in FVB mice by hydrodynamic injection (HDI) using a mutant beta-catenin c-MET transposase system. Serum was collected at 4, 7, 11 and 15 weeks after HDI to assess tumor burden by luciferase activity. Liver tumors were harvested, and stool samples collected from mice with early HCC (luciferase activity < 1,000,000 RLU) or advanced HCC (luciferase activity > 1,000,000 RLU) at 10 weeks or more after HDI. Immunohistochemistry of tissues collected from mice with early HCC (**B**–**D**) and advanced HCC (**E**–**G**) was performed for hematoxylin and eosin (**B** and **E**), CD8 (**C** and **F**) and lipopolysaccharide (**D** and **G**). Scale bars = (**B**–**D**) 500 μm; (**E**–**G**) top panel: 3mm, bottom panel 200 μm.

What is the Phenotype of Tumor Infiltrating Immune Cells?

To determine the immune cell profiles within the liver, we performed high-dimensional single-cell immune phenotyping using mass cytometry (CyTOF) on tissues obtained separately from tumor and non-tumor regions. Non-parenchymal cells were isolated from livers with early stage HCC, where tumor-containing regions could be readily distinguished and separated.

https://doi.org/10.2147/JHC.S524341

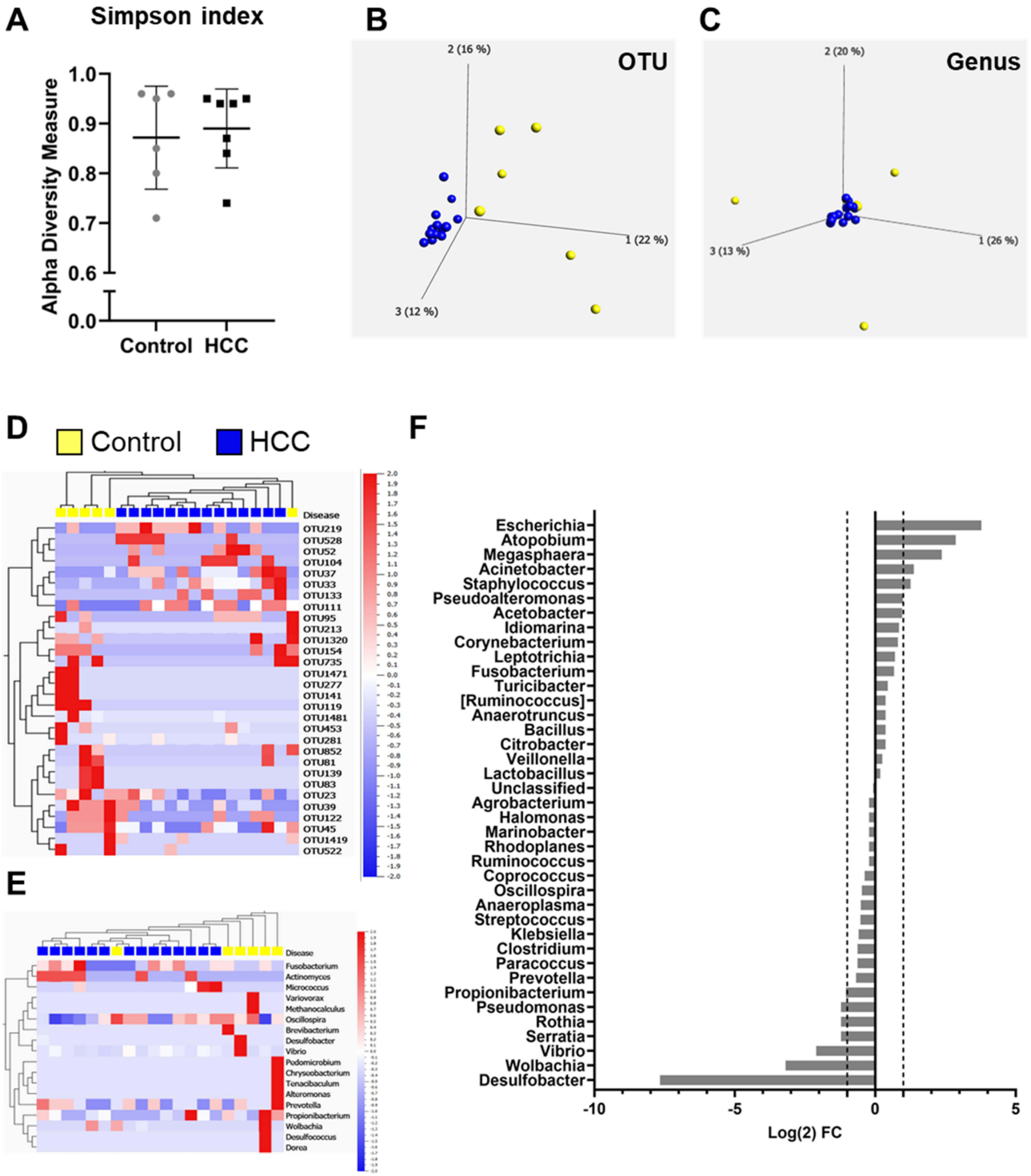

Figure 2 Diversity of tumor-associated hepatic microbiome. Orthotopic HCC and control mouse models were established by hydrodynamic injection using a transposase system with c-MET in combination with mutant beta-catenin (n=7) or c-MET (n=6), respectively. The hepatic microbiome was examined by 16S rRNA sequencing on liver tissue DNA isolated from control livers, or from tumor and adjacent non-tumor tissues from HCC bearing livers. (**A**) Alpha diversity was assessed using the Simpson index. (**B** and **C**) Beta diversity was examined by performing principal component analyses using (**B**) 30 operational taxonomic units (OTU) clusters or (**C**) 18 identified genera. Heat maps of the control and HCC tumor tissue samples were generated to visualize the abundances of the (**D**) OTU clusters and (**E**) genera. (**F**) Differences in the hepatic microbiome between HCC and control livers are represented as the log (2) fold change (FC) in abundance.

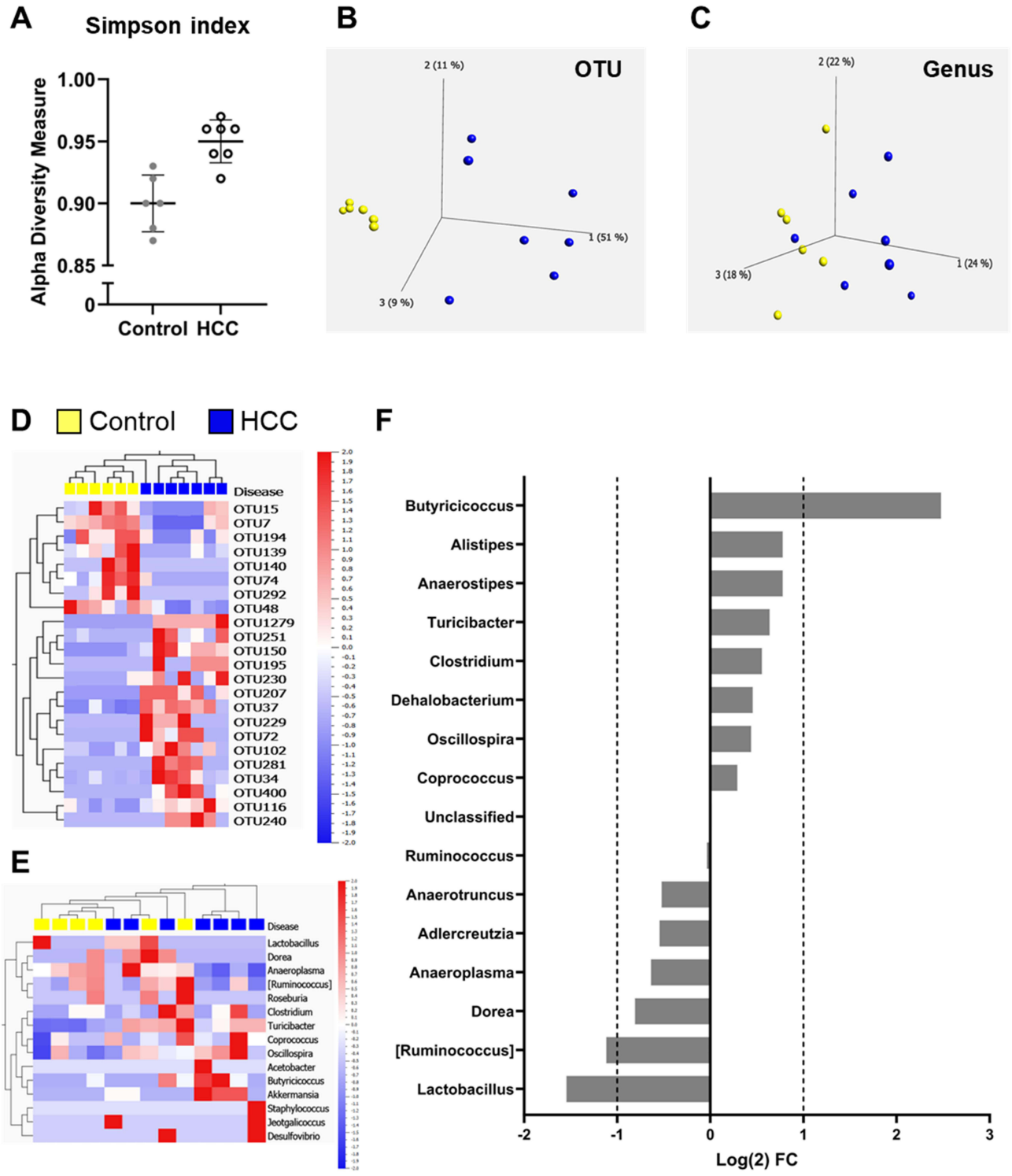

Figure 3 The gut microbiome in tumor bearing and control mice. Orthotopic HCC and control mouse models were established by hydrodynamic injection using a transposase system with c-MET in combination with mutant beta-catenin (n=7) or c-MET (n=6) respectively. Stool samples were collected from control and HCC mice at the study endpoint. DNA extracted from the stool samples was used to perform 16S rRNA sequencing. (**A**) Alpha diversity was assessed using the Simpson index. (**B** and **C**) principal component analysis (PCA) was performed on (**B**) 23 OTU clusters or (**C**) 15 genera. Heatmaps of the (**D**) OTU and (**E**) genera profiles in stool samples from control or HCC bearing mice were generated. (**F**) Differences in the gut microbiome between HCC and control mice are represented as the log (2) fold change (FC) in abundance.

https://doi.org/10.2147/JHC.S524341

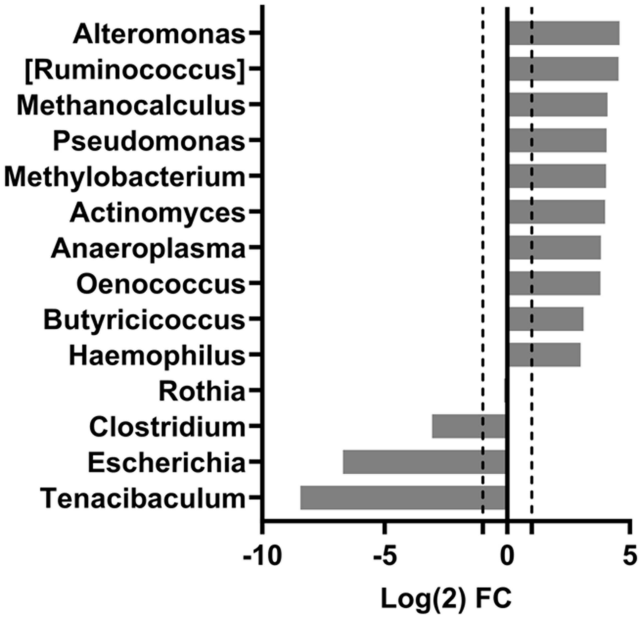

Figure 4 Comparison of tumor and gut microbiomes in mice with HCC. Analysis of hepatic and gut microbiome in mice with experimental HCC induced by expression of mutant beta-catenin. Differences are depicted as the log (2) fold change (FC) between gut and liver microbiomes for all genera showing a greater than 2-fold difference in abundance.

Analysis of the mass cytometry data by manual gating revealed heterogeneity of immune cell distributions within the tumor, as well as in hepatic tissue from non-tumoral regions. An increase in several immune cell subtypes was observed, including markedly elevated levels of $CD4^+$ regulatory T cells () and $CD4^+$ and $CD8^+$ central memory T cells. There were also notable reductions in $CD19^+B220^+$ B cells, neutrophils, $CD4^+$ naïve and effector memory T cells, and $CD8^+$ effector memory T cells in the tumor tissue (Figure 5). These results indicate that tumor-infiltrating immune cells differ from those within resident hepatic tissues and are consistent with immune responses and activation as contributors to TME changes associated with tumor growth or progression.

Does Mutant Beta-Catenin Alter LPS Mediated Signaling?

To generate cells with constitutive β-catenin expression, AML12 murine hepatocytes were transduced with an empty vector or mutant β-catenin vector. The mutant isoform of β-catenin results in constitutive β-catenin expression in hepatocytes. Immunoblot analysis confirmed the successful transduction by demonstrating β-catenin expression (Supplementary Figure 1). Next, we assessed the functional effects of mutant β-catenin on LPS-induced TLR4 signaling in macrophages. Murine macrophages (RAW264.7) were co-cultured with control or β-catenin mutant AML12 cells plated on transwell inserts. The RAW264.7 cells were primed with LPS or left unstimulated before plating. After 48 hours, RAW267.4 cells were harvested, proteins were extracted, and subcellular fractionation was performed. The expression of p65 was assessed in both the cytoplasmic and nuclear compartments. LPS priming reduced the cytoplasmic expression of p65 under both co-culture conditions (Figure 6A). There was a concomitant increase in the nuclear expression of p65 in LPS-primed co-cultured cells compared with that in unstimulated cells (Figure 6B). However, the LPS-induced increase in the nuclear expression of p65 was slightly attenuated when LPS primed RAW264.7 cells were co-cultured with β-catenin mutant AML12 cells. These studies indicated that mutant β-catenin in hepatocytes can block NF-κB translocation and impair LPS-mediated signaling in macrophages.

Does Mutant β-Catenin Modulate Immune Cell Functions Through Alterations in the Tumor Cell Secretome?

The effects of mutant β-catenin on LPS-mediated immune cell signaling in co-culture indicated the involvement of extracellular mediators with alterations in the cellular secretome. Intercellular signaling and modulation of immune cell functions can occur through the release of soluble protein mediators such as chemokines, or through the release of

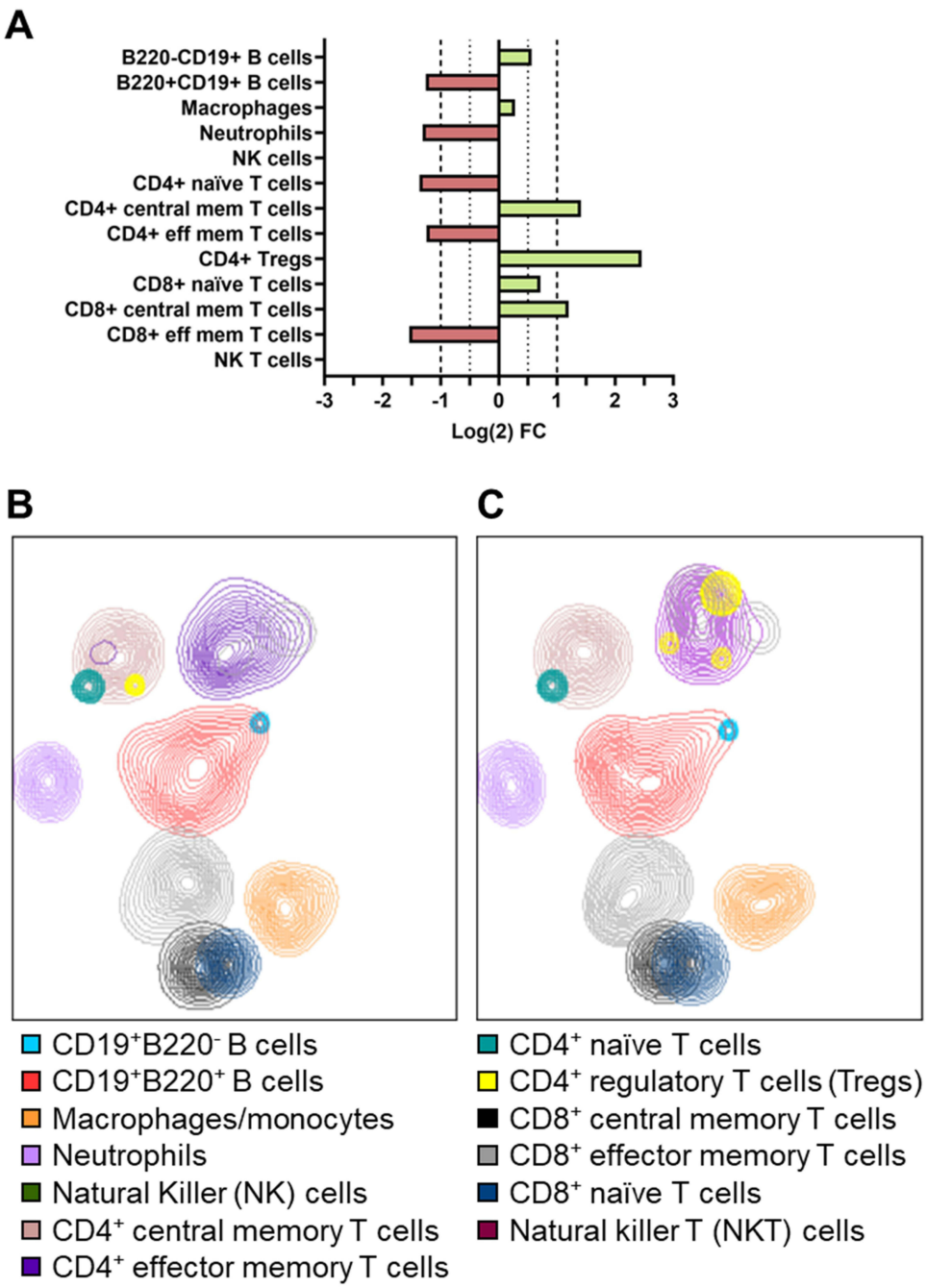

Figure 5 Profiling of the liver cancer immune microenvironment. Tumor and adjacent, non-tumor tissues were harvested from the liver of a mouse with early-stage HCC (luciferase activity < 1,000,000). Hepatic non-parenchymal cells were isolated from the liver tissue samples and mass cytometry was performed to assess the abundance of immune cell subtypes by manual gating. (**A**) Changes in the immune profiles between tumor and adjacent non-tumor liver tissue are depicted as the log (2) fold change (FC, tumor/non-tumor) for each immune cell subtype. The thin and thick dotted lines correspond to log (2) fold change values greater than a magnitude of 0.5 and 1, respectively. Density-independent down-sampling was performed on the samples from tumor tissues to obtain a number of live single $CD45^+$ events that were equivalent to those within the adjacent non-tumor sample. T-SNE plots of the (**B**) non-tumor and (**C**) tumor samples were generated and overlaid with the manually gated cell populations.

extracellular vesicles (EV). First, we evaluated the effect of LPS on the tumor cell secretome in vitro. Secretome profiling was performed using LPS-stimulated macrophages co-cultured with wild-type (WT), mutant β-catenin, or WT hepatocytes. LPS-stimulated co-cultured cells showed reduced secretion of IL-1a ($p<0.005$), IL-1 β ($p<0.0005$), and CXCL10 ($p<0.005$), but the secretion of CXCL9 was significantly increased in mutant β-catenin co-culture conditions ($p<0.05$). (Figure 7A and Supplementary Figure 2). Notably, there was no change in IL-6 levels ($p=0.521$). Next, we examined the secretome profiles of macrophages cocultured with mutant β-catenin or WT hepatocytes. A significant reduction in the

https://doi.org/10.2147/JHC.S524341

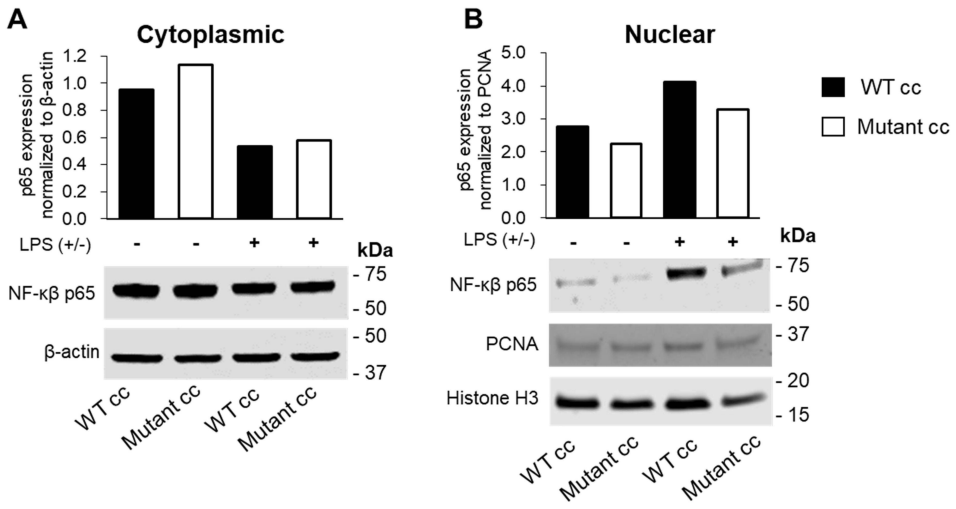

Figure 6 Mutant beta-catenin alters LPS mediated signaling. (**A**) cytoplasmic and (**B**) nuclear proteins were extracted from unstimulated or LPS stimulated RAW264.7 murine macrophages co-cultured (cc) with AML12 murine hepatocytes transfected with control empty vector (WT) or mutant β-catenin (mutant) expression vectors using transwell inserts. Immunoblot analysis was performed for NF-κβ p65, Histone H3, β-actin or PCNA. The quantitative data is represented along with representative blots from three separate determinations.

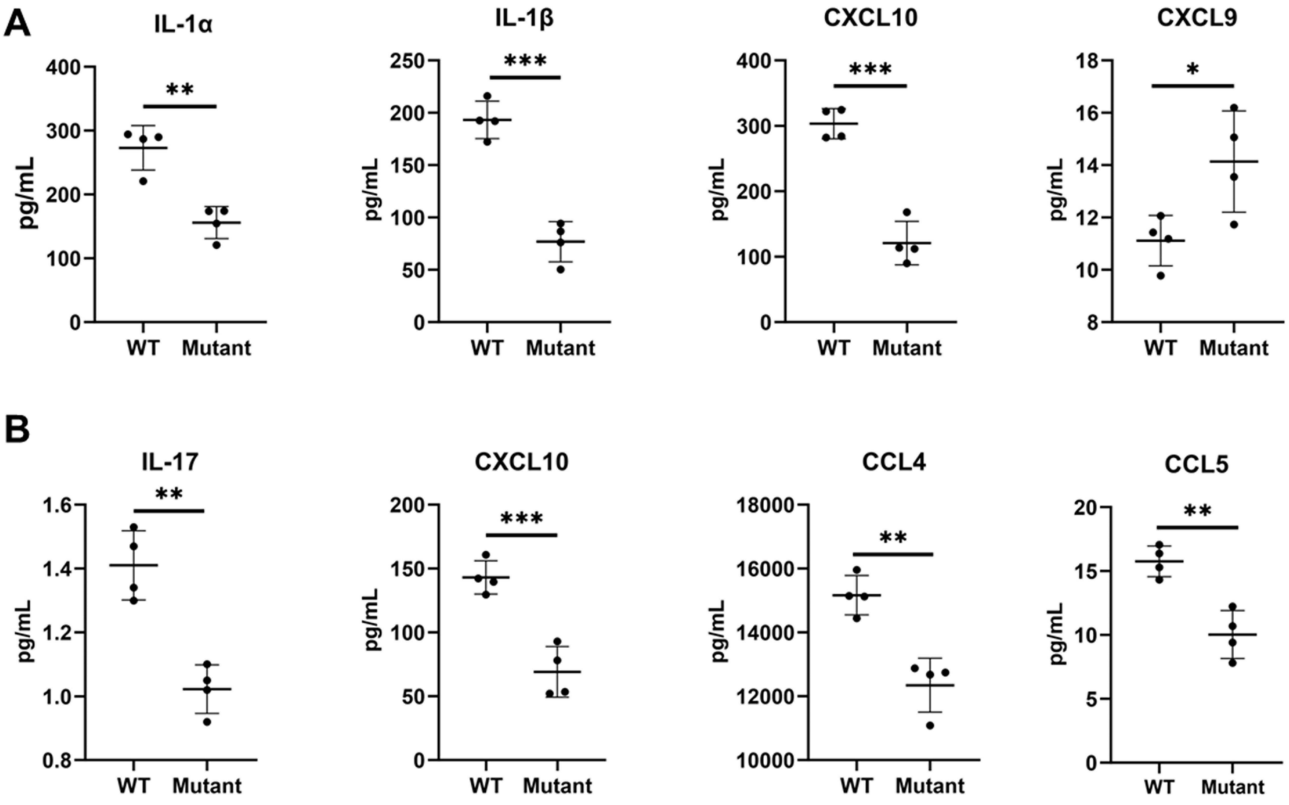

Figure 7 Secretome profiles of macrophages co-cultured with hepatocytes. RAW264.7 murine macrophages were co-cultured with wild type (WT) or β-catenin mutant (Mutant) AML12 murine hepatocytes, and the effects of LPS stimulation on the cellular secretome was evaluated. Soluble protein expression was quantitated in (**A**) LPS-stimulated or (**B**) unstimulated co-cultured cells using an ELISA based assay. The data shown represents the average ± SD from four separate determinations: *p<0.05, **p<0.005, *** p<0.0005.

secretion of several chemokines including CCL4 ($p<0.005$), CCL5 ($p<0.005$) and CXCL10 ($p<0.0.005$) by the co-cultured β-catenin mutant cells, as well as a significant decrease in the secretion of the cytokine, IL-17 ($p<0.005$) (Figure 7B; Supplementary Figure 3). These studies indicate that constitutive β-catenin expression could alter the secretion of immune-modulating chemokines and cytokines, thereby indirectly modulating the activity of immune cells such as cytotoxic T lymphocytes, $CD4^+$ T lymphocytes, NK cells, and neutrophils.

To examine whether tumor cell derived EV could modulate systemic immune profiles, AML murine hepatocytes with constitutive expression of mutant beta-catenin expression (or respective controls) were generated, and co-cultured with RAW264.7 macrophages (LPS stimulated or unstimulated). EV were then isolated from unstimulated or LPS-stimulated macrophages that were mono-cultured (mono EV) or co-cultured with either control or β-catenin-mutant hepatocytes. The size distribution profiles of the EV products were evaluated by nanoparticle tracking analysis (Supplementary Figure 4A–C). Immunoblotting confirmed V5 tag expression in mutant AML12 cell lysate and in EV from the mutant co-cultured cells, verifying expression of the mutant β-catenin in the cells and EV cargo, respectively. In addition, immunoblot analysis confirmed the expression of TSG1010 and CD63, EV markers, in EVs from WT and mutant co-cultured cells (Supplementary Figure 4D). These findings verified that AML12 cells transduced with mutant β-catenin released EV enriched for the mutant β-catenin isoform (Supplementary Figure 5).

Does Mutant Beta-Catenin Alter the Immune Cell Profile in vivo?

To evaluate the immunological effects of β-catenin in vivo, EV derived from monocultured (mono) RAW264.7 cells or RAW264.7 cells co-cultured (cc) with AML12 hepatocytes with wild-type (WT) or mutant β-catenin were injected by tail-vein injection into mice. The spleens were harvested four hours post-injection and immune cell profiling of 15 cell populations was performed. Administration of cc EV WT resulted in marked increases in the frequencies of several subtypes of cytotoxic T lymphocytes within the spleen compared with the response elicited by mono-EV treatment (Figure 8A, Supplementary Table 3). Reductions in the populations of $CD4^+$ Tregs, neutrophils, and $CD19^+B220^-$ B cells were also observed in response to cc EV WT treatment (Figure 3A). To elucidate the immunological impact of β-catenin, we compared the immune profiles of mice treated with WT or cc EV Mutant. Treatment with cc EV Mutant reduced the levels of cytotoxic T lymphocytes as well as $CD4^+$ T cells in the spleen. Increases in NK T cells, neutrophils, and NK cells were also observed in response to cc EV Mutant treatment (Figure 8B, Table 1). Finally, immunomodulatory effects of the microbiome were evaluated. EV isolated from LPS-primed macrophages co-cultured with hepatocytes expressing WT or mutant β-catenin were administered intravenously. A marked increase in the population of $CD4^+$ Tregs was observed in response to treatment with the LPS-primed cc EV Mutant compared to mice treated with LPS-primed cc EV WT (Figure 8C).

Discussion/Conclusion

In this study, we examined the local microenvironmental interplay between oncogenic events and alterations in the tumor microbiome and immune cells within hepatic tumors. These studies have shown that the presence of a definable microbiome within the liver contributes to local microenvironmental changes, and is distinct from the gut microbiome. Within the gut, homeostasis is maintained by the presence of a wide range of microbes and their metabolites. Understanding their contributions to local or systemic effects is the focus of active investigation by many groups. The hepatic parenchyma receives most of its blood supply through the portal vein, and is directly exposed to bacterial products from the gut. The gut microbiome is altered in patients with HCC, and characteristic gut microbial biomarkers have been reported to have a diagnostic utility in patients with early HCC.[15–18] However, our data indicate many differences between the gut and tumor microbiomes in experimentally induced murine HCC. These observations suggest that analysis of the gut microbiome may not adequately reflect or recapitulate the tumor microbiome, and add to the importance of direct hepatic microbiome analysis to understand local microenvironmental influences on tumor growth or therapeutic responses.

Although cancer immunotherapies, including checkpoint blockade antibodies, adoptive T cell therapy, and even some vaccines, have given rise to major clinical responses with durability in many cases, many liver cancers respond poorly. Moreover, a subset of patients who initially respond subsequently develops secondary resistance to therapy. The

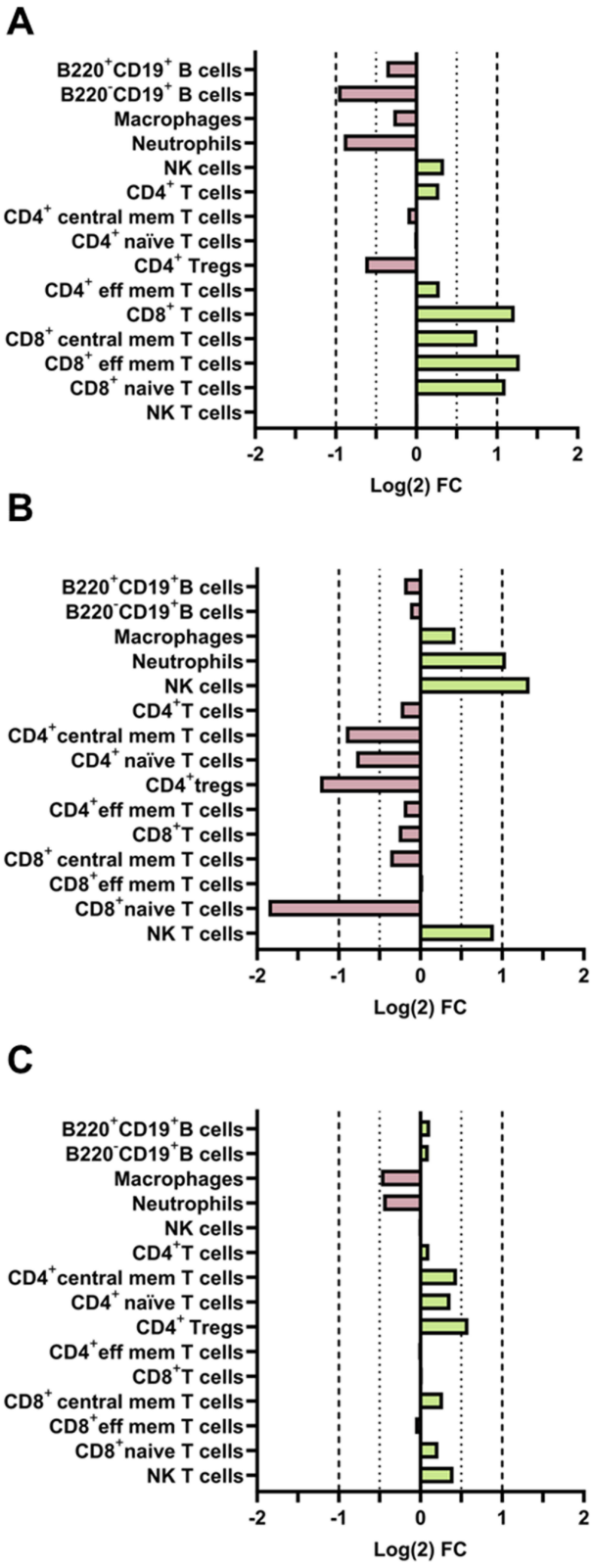

Figure 8 EV mediated changes in immune cell profiles. EVs were isolated from RAW264.7 cells in monoculture (mono EV) or in co-culture with WT (cc EV WT) or mutant β-catenin (cc EV mut) AML12 cells. 1×10^{10} particles of mono EV, cc EV WT or cc EV mut were injected by tail vein injection. After four hours the spleens were harvested, single cell suspensions of the splenocytes were prepared and used for mass cytometry. Manual gating was used to identify immune cell subtypes. Differences in immune cell subtype frequencies are represented as log (2) fold change between groups following administration of EV from. (**A**) mono EV and cc EV WT; (**B**) cc EV WT and cc EV mut and (**C**) LPS stimulated cc EV WT and LPS stimulated cc EV mut.

Table 1 Immune Cell Frequencies

Cell Subtypes	cc EV WT	cc EV mut	Log_2 Fold Change (mut/WT)
$B220^+$ $CD19^+$ B cells	30.5	26.6	−0.2
$B220^-$ $CD19^+$ B cells	2.1	1.9	−0.13
Macrophages	11.9	16.1	0.43
Neutrophils	1.9	4.0	1.05
NK cells	2.2	5.6	1.35
$CD4^+$ T cells	19.8	16.8	−0.24
$CD4^+$ naïve T cells	0.3	0.2	−0.79
$CD4^+$ central memory T cells	1.8	1.0	−0.91
$CD4^+$ effector memory T cells	13.0	11.3	−0.20
CD4+ Tregs	0.5	0.2	−1.23
$CD8^+$ T cells	21.0	17.5	−0.27
$CD8^+$ naïve T cells	0.7	0.2	−1.86
$CD8^+$ central memory T cells	1.3	1.0	−0.37
$CD8^+$ effector memory T cells	7.0	6.9	−0.01
NK T cells	0.1	0.1	0.90

Notes: Frequencies of immune cells in the spleens of mice following systemic administration of extracellular vesicles isolated from unstimulated RAW264.7 cells co-cultured with wild type (cc EV WT) or mutant β-catenin (cc EV mut) AML12 cells.

mechanisms of therapeutic resistance are diverse and can involve tumor-intrinsic mechanisms as well as alterations in the tumor environment and microbiome. Our results suggest that resistance to immunotherapies can result from the emergence of new oncogenic variants that mediate T cell exclusion, such as activating mutations in β-catenin. In addition to mutations in β-catenin, mutations in several other tumor cell oncogenes have been shown to underlie immune exclusion through their effects on immune cells.[8] Among these are the loss of PTEN, activation of PPAR, and activating mutations in FGFR3.[19–21] Such tumor-specific oncogenic alterations can be associated with or result in alterations within the tumor microbiome or microenvironment that can independently modulate therapeutic responses. Further studies are warranted to elucidate the targeted effects of oncogenic mutations on the tumor microbiome, as these may provide further opportunities for improving therapeutic responses.

Intestinal dysbiosis is prevalent in patients with HCC and underlying cirrhosis. Toxic factors arising from alterations in the gut microbiota include damage- and pathogen-associated molecular patterns. Gut dysbiosis and disruption of intestinal permeability results in the translocation of these metabolites and their delivery to the liver through the portal vein. Can targeting the gut microbiota modulate HCC risk or improve response to therapy? A reduction in HCC formation has been reported in different experimental models of HCC with manipulation of the gut-liver microbiome. For example, an increase in HCC has been reported in studies involving gut-sterilized and germ-free mice, mice treated with microbial metabolites (MAMPs), and mice following disruption of the gut barrier (eg, with dextran sulfate sodium). However, these perturbations may be associated with increased systemic LPS levels and liver fibrosis, which could independently increase HCC, but their impact on the hepatic microbiome is unknown. Nevertheless, these observations suggest that targeting the gut microbiota may be a feasible therapeutic addition to manipulating the hepatic microbiome

and TME to modulate the response to immune or other therapeutic approaches for HCC. This is important with the advent of immunotherapy-based first-line regimens for HCC treatment.

Our data provide a strong rationale for further studies to understand the interplay between the tumor microbiome, genetic mutations, and immunity, which could ultimately result in the development of therapeutic approaches to modulate these processes with the aim of restoring immune cell infiltration and augmenting responses to immunotherapy within the TME.

Abbreviations

CCL, chemokine C-C motif ligand; CXCL, C-X-C motif chemokine ligand; CyTOF, cytometry by time-by-flight; EV, extracellular vesicles; FGFR, fibroblast growth factor receptor; HCC, hepatocellular cancer; H&E, hematoxylin and eosin; IL, interleukin; IP, intraperitoneal; IV, intravenous; LPS, lipopolysaccharide; MAMP, microbe-associated molecular pattern; NF-κβ, nuclear factor kappa light chain enhancer of activated B cells; NK, natural killer T cells; NTA, nanoparticle tracking analysis; LPS, lipopolysaccharide; PD-L, programmed death ligand; PCA, principle component analysis; PPAR, peroxisome proliferator-activated receptor; PTEN, phosphatase and tensin homolog; OTU, operational taxonomic units; TFF, tangential flow filtration; TLR, toll-like receptor; TME, tumor microenvironment; TNF-α, tumor necrosis factor-α; TSG, tumor susceptibility gene; Tregs, regulatory T cells.

Data Sharing Statement

All data generated or analyzed during this study are included in this article and its Supplementary Material Files or are available upon request. Further inquiries can be directed to the corresponding author.

Statement of Ethics

This study was reviewed and approved by the Mayo Clinic Institutional Animal Care and Use Committee (approval protocol A00005435).

Acknowledgment

This work was supported by an NIH grants CA217833 to (TP). We acknowledge the helpful discussions by all other members of the Patel lab and the assistance provided by the Cell & Tissue Analysis Shared Resource Laboratory, Mayo Clinic, Jacksonville, FL.

Author Contributions

All authors made a significant contribution to the work reported, whether that is in the conception, study design, execution, acquisition of data, analysis and interpretation, or in all these areas; took part in drafting, revising or critically reviewing the article; gave final approval of the version to be published; have agreed on the journal to which the article has been submitted; and agree to be accountable for all aspects of the work.

Funding

This work was supported by an NIH grant (CA217833) to TP.

Disclosure

The authors report no conflicts of interest in this work.

References

1. Binnewies M, Roberts EW, Kersten K, et al. Understanding the tumor immune microenvironment (TIME) for effective therapy. *Nat Med*. 2018;24(5):541–550. doi:10.1038/s41591-018-0014-x
2. Harding JJ, Nandakumar S, Armenia J, et al. Prospective genotyping of hepatocellular carcinoma: clinical implications of next-generation sequencing for matching patients to targeted and immune therapies. *Clin Cancer Res*. 2019;25(7):2116–2126. doi:10.1158/1078-0432.CCR-18-2293
3. Spranger S, Bao R, Gajewski TF. Melanoma-intrinsic β-catenin signalling prevents anti-tumour immunity. *Nature*. 2015;523(7559):231–235. doi:10.1038/nature14404

4. Bonaventura P, Shekarian T, Alcazer V, et al. Cold tumors: a therapeutic challenge for immunotherapy. *Front Immunol*. 2019;10:168. doi:10.3389/fimmu.2019.00168
5. Pinyol R, Sia D, Llovet JM. Immune exclusion-Wnt/CTNNB1 class predicts resistance to immunotherapies in HCC. *Clin Cancer Res*. 2019;25(7):2021–2023. doi:10.1158/1078-0432.CCR-18-3778
6. Thorsson V, Gibbs DL, Brown SD, et al. The Immune Landscape of Cancer. *Immunity*. 2019;51(2):411–412. doi:10.1016/j.immuni.2019.08.004
7. Luke JJ, Bao R, Sweis RF, et al. WNT/β-catenin pathway activation correlates with immune exclusion across human cancers. *Clin Cancer Res*. 2019;25(10):3074–3083. doi:10.1158/1078-0432.CCR-18-1942
8. Grasso CS, Giannakis M, Wells DK, et al. Genetic mechanisms of immune evasion in colorectal cancer. *Cancer Discov*. 2018;8(6):730–749. doi:10.1158/2159-8290.CD-17-1327
9. Spranger S, Luke JJ, Bao R, et al. Density of immunogenic antigens does not explain the presence or absence of the T-cell-inflamed tumor microenvironment in melanoma. *Proc Natl Acad Sci U S A*. 2016;113(48):E7759–e7768. doi:10.1073/pnas.1609376113
10. Sia D, Jiao Y, Martinez-Quetglas I, et al. Identification of an immune-specific class of hepatocellular carcinoma, based on molecular features. *Gastroenterology*. 2017;153(3):812–826. doi:10.1053/j.gastro.2017.06.007
11. Matsuda A, Ishiguro K, Yan IK, et al. Therapeutic efficacy of Vitamin D in experimental c-MET-β-catenin-driven hepatocellular cancer. *Gene Expr*. 2019;19(2):151–159. doi:10.3727/105221618X15355518848281
12. Andersen MN, Al-Karradi SNH, Kragstrup TW, et al. Elimination of erroneous results in flow cytometry caused by antibody binding to Fc receptors on human monocytes and macrophages. *Cytometry A*. 2016;89(11):1001–1009. doi:10.1002/cyto.a.22995
13. Matsuda A, Ishiguro K, Yan IK, et al. Extracellular vesicle-based therapeutic targeting of β-catenin to modulate anticancer immune responses in hepatocellular cancer. *Hepatol Commun*. 2019;3(4):525–541. doi:10.1002/hep4.1311
14. Ishiguro K, Yan IK, Lewis-Tuffin L, et al. Targeting liver cancer stem cells using engineered biological nanoparticles for the treatment of hepatocellular cancer. *Hepatol Commun*. 2020;4(2):298–313. doi:10.1002/hep4.1462
15. Ponziani FR, Bhoori S, Castelli C, et al. Hepatocellular carcinoma is associated with gut microbiota profile and inflammation in nonalcoholic fatty liver disease. *Hepatology*. 2019;69(1):107–120. doi:10.1002/hep.30036
16. Ren Z, Li A, Jiang J, et al. Gut microbiome analysis as a tool towards targeted non-invasive biomarkers for early hepatocellular carcinoma. *Gut*. 2019;68(6):1014–1023. doi:10.1136/gutjnl-2017-315084
17. Grąt M, Wronka KM, Krasnodębski M, et al. Profile of gut microbiota associated with the presence of hepatocellular cancer in patients with liver cirrhosis. *Transplant Proc*. 2016;48(5):1687–1691. doi:10.1016/j.transproceed.2016.01.077
18. Liu Q, Li F, Zhuang Y, et al. Alteration in gut microbiota associated with hepatitis B and non-hepatitis virus related hepatocellular carcinoma. *Gut Pathog*. 2019;11(1):1. doi:10.1186/s13099-018-0281-6
19. George S, Miao D, Demetri GD, et al. Loss of PTEN is associated with resistance to anti-PD-1 checkpoint blockade therapy in metastatic uterine leiomyosarcoma. *Immunity*. 2017;46(2):197–204. doi:10.1016/j.immuni.2017.02.001
20. Peng W, Chen JQ, Liu C, et al. Loss of PTEN promotes resistance to T cell-mediated immunotherapy. *Cancer Discov*. 2016;6(2):202–216. doi:10.1158/2159-8290.CD-15-0283
21. Sweis RF, Spranger S, Bao R, et al. Molecular drivers of the non-T-cell-inflamed tumor microenvironment in urothelial bladder cancer. *Cancer Immunol Res*. 2016;4(7):563–568. doi:10.1158/2326-6066.CIR-15-0274